Smart Structures and Systems, *Vol. 31, No. 6 (2023) 545-559*
https://doi.org/10.12989/sss.2023.31.6.545

Optimal sensor placement of retrofitted concrete slabs with nanoparticle strips using novel DECOMAC approach

Ali Faghfouri*[1], Hamidreza Vosoughifar [2a] and Seyedehzeinab Hosseininejad [3b]

[1] *Institute of Environmental Sciences, Université du Québec à Montréal, C.P. 8888, succursale Centre-ville, Montréal, Québec, H3C 3P8, Canada*
[2] *Department of Civil and Environmental Engineering and Water Resources Research Center, University of Hawaii at Manoa. 2540 Dole Street, Holmes 342, Honolulu, Hawaii 96822, USA*
[3] *Department of Civil Engineering, Islamic Azad University, Tehran South Branch, 1777613651, Tehran, Iran*

(*Received April 10, 2022, Revised March 25, 2023, Accepted May 1, 2023*)

Abstract. Nanoparticle strips (NPS) are widely used as external reinforcers for two-way reinforced concrete slabs. However, the Structural Health Monitoring (SHM) of these slabs is a very important issue and was evaluated in this study. This study has been done analytically and numerically to optimize the placement of sensors. The properties of slabs and carbon nanotubes as composite sheets were considered isotopic and orthotropic, respectively. The nonlinear Finite Element Method (FEM) approach and suitable optimal placement of sensor approach were developed as a new MATLAB toolbox called DECOMAC by the authors of this paper. The Suitable multi-objective function was considered in optimized processes based on distributed ECOMAC method. Some common concrete slabs in construction with different aspect ratios were considered as case studies. The dimension and distance of nano strips in retrofitting process were selected according to building codes. The results of Optimal Sensor Placement (OSP) by DECOMAC algorithm on un-retrofitted and retrofitted slabs were compared. The statistical analysis according to the Mann-Whitney criteria shows that there is a significant difference between them (mean P-value = 0.61).

Keywords: carbon nanotube; DECOMAC algorithm; Nanoparticle strips; Structural Health Monitoring; two-way reinforced concrete slabs

1. Introduction

Structural Health Monitoring (SHM) is a continuous measurement system used to monitor the status of structures. It involves measuring various structural quantities and can be used to evaluate the design and construction process. The results obtained through SHM can help in identifying critical points and determining more efficient means of retrofitting. The use of SHM can significantly reduce the likelihood of damage, ultimately improving the overall safety of the structure. The SHM technique finds widespread application in the retrofitting process. In recent years, composite materials, such as carbon, basalt, glass, and aramid fiber reinforced polymer (FRP), have increasingly been utilized for retrofitting slabs. Fernandes *et al*. (2017) investigated RC slabs with reinforced concrete on the tensile strength. The study involved the measurement of horizontal shear stress and the growth of two-directional shear specimens to assess cracks on the slabs. Kaveh *et al*. (2016) introduced a modified particle swarm optimization (PSO) algorithm called probabilistic particle swarm optimization (PPSO) for the optimal design of large-span prestressed concrete slabs. The study evaluated the algorithm's robustness by comparing its performance with PSO and harmony search using a large-span prestressed concrete slab model generated in SAP2000. Results show that PPSO outperformed the other algorithms, converged faster, and produced lower weight. Overall, the study suggested that PPSO is a promising approach for the optimal design of large-span prestressed concrete slabs. Herraiz and Vogel (2016) investigated a new method for unbound concrete slabs through membrane behavior analysis. In this study, 43 experimental tests were used to compare the proposed approach with other methods. The comparison revealed a strong correlation between the model predictions and reference results, indicating the effectiveness of the proposed method. Khajehdehi and Panahshahi (2016) conducted a study to investigate the behavior of concrete slabs with and without openings. The study aimed to explore the positive contribution of reinforced bars at the corners of the openings in enhancing the capacity of panels with openings, using FEM. Thiagarajan *et al*. (2015) conducted an experimental and numerical analysis of reinforced concrete slabs subjected to blast loads. In this study, the mesh sensitivity, depth, and mouth of cracks were also considered. Mosalam and Mosallam (2001) researched on the difference of concrete

*Corresponding author, Ph.D. Candidate,
E-mail: faghfouri.ali@courrier.uqam.ca
[a] Ph.D., Professor,
E-mail: Vosoughi@hawaii.edu
[b] Ph.D. Student,
E-mail: SZHosseininejad@gmail.com

ISSN: 1738-1584 (Print), 1738-1991 (Online)

damage between built and retrofitted slabs using nonlinear transient analysis retrofitted with CFRP composites. The study concluded that the CFRP composite retrofit system can increase the load-bearing capacity of the slabs while minimizing the damage phenomenon in concrete. Maheri *et al*. (2019) conducted numerical studies on full-scale unreinforced concrete block masonry walls, retrofitted by reinforced concrete layers to determine their in-plane shear capacity. Nonlinear pushover analyses were performed to investigate the effects of various problematic variables on the performance of the retrofitted walls. The findings of the study have important implications for the design and retrofitting of masonry walls, highlighting the need to carefully consider boundary conditions to improve the performance and safety of such structures. Ma *et al*. (2017) researched on the seismic performance of reinforced concrete (RC) frames and the impact of carbon fiber-reinforced polymer (CFRP) retrofitting on their failure modes. The main outcome of this research was an increase in the failure mode, ductility, and energy dissipation capacity of the CFRP retrofitted beam-column-slab. Guo *et al*. (2017) proposed a retrofitting method aimed at enhancing the blast resistance of reinforced concrete (RC) slabs against conventional explosions by utilizing externally bonded glass fiber reinforced polymer (GFRP) strips. Their study demonstrated that strengthening RC slabs with bonded GFRP strips can significantly improve the ultimate blast-resistant capacity of slabs against conventional explosive blasts. Afefy *et al*. (2019) developed experimental research on strengthening techniques for defected reinforced-concrete cantilever slabs. Their study focused on the use of bonded carbon fiber-reinforced polymer sheets to restore lost flexural capacities that resulted from insufficient bond length of the main tensile steel. The experimental findings revealed that the strengthening technique based on embedded steel bars was highly effective in restoring the slab's lost capacity. In fact, the strengthened slab using this technique performed even better than a properly detailed slab, with an improvement of approximately 5%. Overall, the study suggests that incorporating embedded steel bars in strengthening techniques can significantly enhance the flexural capacity of reinforced-concrete cantilever slabs and may serve as an effective solution for restoring lost capacity. Navarro *et al*. (2018) conducted a study on the parametric computational analysis of punching shear in reinforced concrete (RC) slabs, both with and without opening. The study's findings demonstrate that the yield point strength of bars can increase the ultimate load of the slab and decreases the final displacement. The FRPs possess numerous advantages, among which are their high tensile strength, corrosion resistance and lightness. The advantages of nanocomposite materials make them a versatile option for various engineering applications. Notably, their ease of use and installation, exceptional resistance to high temperatures, as well as resistance to severe mechanical and environmental conditions, make them a highly desirable choice. Kang *et al*. (2006) researched on strain sensors in the SHM issue of carbon nanotube. The researchers utilized a polymer material consisting of carbon nanotubes to fabricate a highly effective strain sensor specifically designed for SHM purposes. Konka *et al*. (2013) carried out a crucial investigation into the implementation of sensors within composite structures for monitoring stress/strain levels at critical points. The researchers employed modal analysis to detect OSP of these structures. Wang (2013) studied the non-destructive evaluation (NDE) capabilities of carbon nanotubes (CNTs) of various network architectures for SHM purposes. The study involved testing three different types of laminate samples with different CNT network architectures in open-hole tension. The results revealed that the consistency and effectiveness of indicating damage accumulation varied significantly based on the CNT network architecture employed. Tan *et al*. (2011) conducted a thorough investigation on the fabrication of composite sensors based on CNTs for SHM. The objective of their research was to develop a cutting-edge sensor capable of accurately detecting strain in structures by measuring the electrical impedance of the CNT composite. Bekas *et al*. (2015) investigated SHM of CNT. Their research was focused on the development of an innovative technique known as Electrical Potential Mapping (EPM) that could effectively detect any damage in CNT composite materials. Sengezer and Seidel (2017) researched the application of in situ SHM in polymer-bonded materials. Wang *et al*. (2018) introduced carbon nanomaterials that enabled fiber sensors for in situ SHM of polymeric composites. The study focused on developing self-sensing composites, which could be achieved through various integration strategies. These strategies included the use of carbon nanotube (CNT) coated fibers (CNTF), reduced graphene oxide (RGO) coated fibers (RGOF), and carbon fibers (CF). Lu *et al*. (2018) researched on behaviors of strain sensors and health monitoring for composite materials. The findings of their research unequivocally demonstrate that strain sensors are highly useful for detecting damage in composite structures. Extensive research has been conducted on SHM using various techniques such as system identification, Hybrid FEM-GA Technique, MAC, minMAC, EI, COMAC, etc. In these studies, sensors were installed to collect crucial structural information. Following stress analysis, the collected data can be utilized to identify critical locations and assess the overall health of the structure. The most widely used OSP approach is the modal assurance criterion (MAC) algorithm. Yi *et al*. (2016) developed an OSP approach in a sensor network that was designed to SHM of a Building. They found that adding one more sensor at each stage of analysis was necessary until the maximum off-diagonal element of the MAC reached a predetermined threshold. The coordinate modal assurance criterion (COMAC) was defined based on the original MAC. Vosoughifar and Khorani (2019) investigated the OSP of RCC Dams using the COMAC approach. In this novel study, the placement of smart sensors was accurately estimated. Vosoughifar *et al*. (2012) proposed OSP for steel structures with a unbonded braced frame (UBF) system for SHM. This paper employed three different OSP methods, with a Genetic Algorithm (GA) selected as the optimization solution to determine the optimal sensor placement based on the structural dynamic response of the UBF system. The

results indicate that a well-designed OSP algorithm for SHM in UBF structures enables the identification of weak and vulnerable points more effectively than when a UBF system is not employed. Shokouhi and Vosoughifar (2013) proposed a new OSP method in the lightweight framing structures using the novel TTFD approach. The study incorporated the use of three distinct OSP methods, ultimately selecting the Genetic Algorithm (GA) as the optimal solution for the optimization formulation to determine the most effective sensor placement based on the dynamic response of the LSF system. Kaveh and Dadras Eslamlou (2019) proposed a new algorithm called QWSA for optimizing sensor placement in structures with multiple candidate locations. QWSA incorporates the Q-learning algorithm into the binary water strider algorithm and employs the tridimensional modal assurance criterion (TMAC) as its objective function. The proposed method was compared with other metaheuristics in the literature on two dome-shaped trusses, and the results showed that QWSA outperforms other methods in terms of cost value, convergence speed, and the triaxial driving-point residue (DPR3) coefficient. It is concluded that QWSA provides an effective solution for optimizing sensor placement in structures with multiple candidate locations. A review of past studies on SHM of slabs shows that one of the main problems in the OSP process is the consideration of line-by-line methods based on MAC, COMAC or ECOMAC methods to optimize sensor placement. The main advantage of this study is to consider a distributed approach in the OSP process rather than a line-by-line approach.

2. Mathematical model

Fig. 1 illustrates a schematic concrete slab retrofitted with carbon nanotubes. The contact element between concrete and nanocomposite material was considered based on the Pasternak model. This model includes an infinite set of springs and dashpots in parallel and supports recovery and creep features well.

The mechanical model of nanocomposite elements with a Pasternak foundation was meticulously evaluated by Eringen and Edelen (1972), utilizing the nonlocal elasticity theory. As per this theory, the stress tensor at the desired point in a nanocomposite material depends on the strain at this point and all other points of this element. According to this theory, the constructive equation for a homogeneous linear nonlinear tensile body with neglect of body forces is given as Eq. (1).

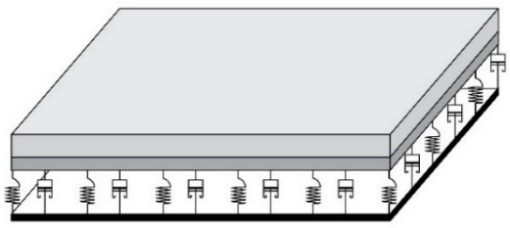

Fig. 1 Retrofitted concrete slab with carbon nanotubes under compressive axial load

$$\sigma_{ij}^{nl}(x) = \int_V \alpha(|x-x'|,\tau)|\sigma_{ij}^{l}\, dV\,(x') \quad \forall x\epsilon \cdot V$$
$$\tau = \frac{e_0 a}{l} \tag{1}$$

Where σ_{ij}^{nl} and σ_{ij}^{l} are nonlocal and local stress tensors respectively, the term $\alpha(|x-x'|,\tau)|$ represents the nonlocal modulus, $|x-x'|$ shows the distance between x and x'. The l, a and e_0 are external characteristic length, internal characteristic length of the material and constant parameter, respectively. These variables were obtained from the experimental study. The simple form of Eq. (1) is given as Eq. (2).

$$(1-\mu\nabla^2)\sigma^{nl} = C\varepsilon$$
$$\mu = (e_0 a)^2 \tag{2}$$

Where μ shows the small-scale effect on the response of the plates in Nano size, and ∇^2 is the Laplacian operator in a Cartesian coordinate system. Moreover, C is the fourth-order stiffness tensor and ε is the strain. The matrix form of Eq. (2) for the orthotropic Nano-plate, can be written as Eq. (3).

$$\begin{Bmatrix}\sigma_{xx}^{nl}\\ \sigma_{yy}^{nl}\\ \sigma_{yz}^{nl}\\ \sigma_{xz}^{nl}\\ \sigma_{xy}^{nl}\end{Bmatrix} - \mu\nabla^2\begin{Bmatrix}\sigma_{xx}^{nl}\\ \sigma_{yy}^{nl}\\ \sigma_{yz}^{nl}\\ \sigma_{xz}^{nl}\\ \sigma_{xy}^{nl}\end{Bmatrix} = \begin{bmatrix}C11 & C12 & 0 & 0 & 0\\ C21 & C22 & 0 & 0 & 0\\ 0 & 0 & C44 & 0 & 0\\ 0 & 0 & 0 & C55 & 0\\ 0 & 0 & 0 & 0 & C66\end{bmatrix}\begin{Bmatrix}\varepsilon_{xx}^{nl}\\ \varepsilon_{yy}^{nl}\\ \varepsilon_{yz}^{nl}\\ \varepsilon_{xz}^{nl}\\ \varepsilon_{xy}^{nl}\end{Bmatrix} \tag{3}$$

In Eq. (3), *Cij* values depend on the orthotropic Nano-plate properties and can be express as Eq. (4).

$$C_{11} = \frac{E_1}{1-v_{12}v_{21}}, \quad C_{12} = \frac{v_{12}E_2}{1-v_{12}v_{21}},$$
$$C_{22} = \frac{E_2}{1-v_{12}v_{21}}, \quad C66 = G23,$$
$$C44 = G13, \quad C55 = G12 \tag{4}$$

Where *E*, *G* and *v* are the Young module, shear module and the Poisson's ratio, respectively.

Mid-plate theory was utilized to estimate shear deformation and rotational effects. This theory is suitable for developing governing equations for composite plates. In this theory, (U_0, V_0, W_0), (∅x, ∅y) and (U, V, W) are the intermediate surface displacements, the intermediate surface rotations and the displacement components of an arbitrary point, respectively. These variables can be calculated using Eq. (5).

$$U(x,y,z,t) = U_0(x,y,t) + Z\,\emptyset\, x(x,y,t)$$
$$V(x,y,z,t) = V_0(x,y,t) + Z\,\emptyset\, y(x,y,t)$$
$$W(x,y,z,t) = W_0(x,y,t) \tag{5}$$

Where t in above equation represents the time of simulation. The in-plane and transverse shear strains of the composite plane are given in Eq. (6).

$$\begin{Bmatrix}\varepsilon xx\\ \varepsilon yy\\ \gamma xy\end{Bmatrix} = \begin{Bmatrix}\varepsilon_{xx}^{(0)}\\ \varepsilon_{yy}^{(0)}\\ \gamma_{xy}^{(0)}\end{Bmatrix} + Z\begin{Bmatrix}\varepsilon_{xx}^{(1)}\\ \varepsilon_{yy}^{(1)}\\ \gamma_{xy}^{(1)}\end{Bmatrix}, \quad \begin{Bmatrix}\gamma_{yz}\\ \gamma_{xz}\end{Bmatrix} = \begin{Bmatrix}\gamma_{yz}^{(0)}\\ \gamma_{xz}^{(0)}\end{Bmatrix} \tag{6}$$

Where,

$$\begin{Bmatrix} \varepsilon_{xx}^{(0)} \\ \varepsilon_{yy}^{(0)} \\ \gamma_{xy}^{(0)} \end{Bmatrix} = \begin{Bmatrix} U_{0,x} \\ v_{0,y} \\ U_{0,x} + v_{0,y} \end{Bmatrix} \begin{Bmatrix} \varepsilon_{xx}^{(1)} \\ \varepsilon_{yy}^{(1)} \\ \gamma_{xy}^{(1)} \end{Bmatrix} = \begin{Bmatrix} \emptyset x, x \\ \emptyset y, y \\ \emptyset x, x + \emptyset y, y \end{Bmatrix}, \quad (6)$$

$$\begin{Bmatrix} \gamma_{yz}^{(0)} \\ \gamma_{xz}^{(0)} \end{Bmatrix} = \begin{Bmatrix} \emptyset y + w_{0,y} \\ \emptyset x + w_{0,x} \end{Bmatrix}$$

3. Modeling

A series of nonlinear FEM analysis were used to obtain the modal shapes and seismic behavior of the selected slabs. Previous research on structural damage identification has demonstrated a limited number of studies that investigate the actual seismic behavior of structures during OSP processes. In this regard, the novel ECOMAC approach was proposed as a suitable and comprehensive method to detect the location of sensors in un-retrofitted and retrofitted slabs.

3.1 Modal analysis

The modal analysis of the selected case studies was carried out to obtain natural frequencies and mode shapes. The mass participation ratio of the necessary modes should not be less than 90% of the total mass of the concrete slabs according to the seismic codes.

In the selected slabs, only eight modes have 90% mass participation, and these effective modes were considered to obtain MAC, COMAC and ECOMAC values.

3.2 MAC and other related methods

Vandiver (1977) combined the results of the eigenvector with FEM analysis to propose the MAC approach. The MAC algorithm can establish the relationship between the effective state mode shapes. In fact, this method was used to make a relation between each two vectors of effective mode shapes. When two mode shapes are in the same or close direction, the MAC value or correlation coefficient will be

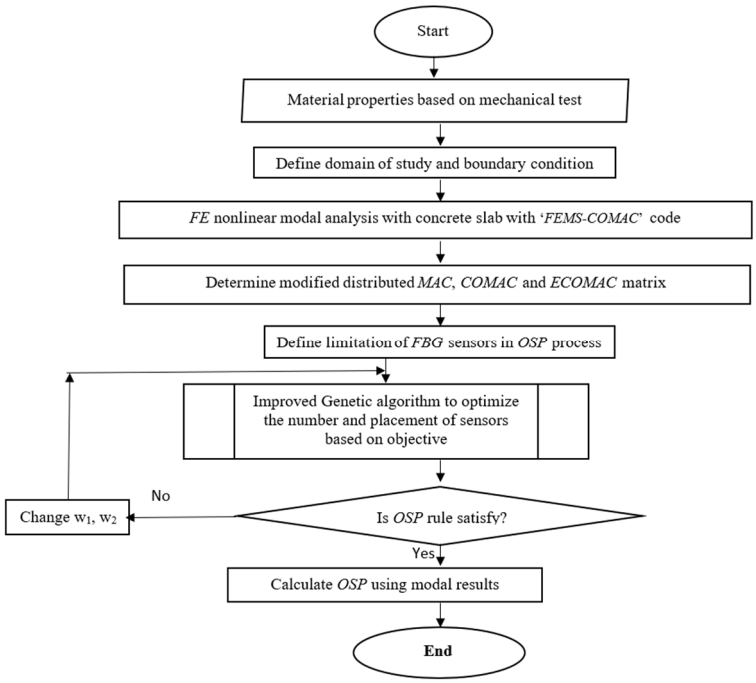

(a) Main algorithm of distributed ECOMAC

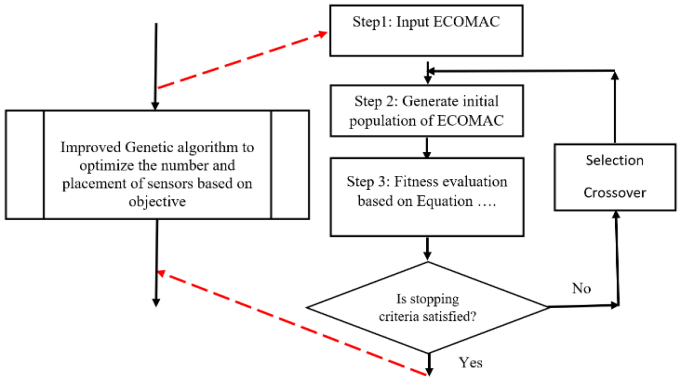

(b) Subroutine of genetic algorithm

Fig. 2 The flowchart of FEMS-ECOMAC code

equal or close to one. Conversely, when there is a significant difference between the two mode shapes, the correlation between them will be less in the off-diagonal element of the MAC matrix. In other words, the MAC approach serves as a mathematical criterion to assess the compatibility between two eigenvectors. Eq. (7) gives the MAC equation.

$$\mathrm{MAC} = \frac{\left(\varphi_i{}^T \varphi_j\right)^2}{\left(\varphi_i{}^T \varphi_j\right)\left(\varphi_j{}^T \varphi_i\right)} \tag{7}$$

The OSP approach has been specifically designed to effectively identify structural weak points that are susceptible to damage. Coppolino and Rubin (1980) proposed the COMAC approach which takes into account point coordination in the MAC algorithm. This method can be obtained based on a set of pairs between analytical, experimental and numerical data. Eq. (8) gives the COMAC formula.

$$\mathrm{COMAC} = \frac{[\sum_{i=1}^{N} |\{\varphi_i\}\{\varphi_i^*\}|]^2}{\sum_{i=1}^{N}(\{\varphi_i\}^2)\ \sum_{i=1}^{N}(\{\varphi_i{}^*\})^{\,2}} \tag{8}$$

Hunt *et al*. (1990) evaluated the new OSP method to address issues stemming from defective scaling, calibration, or placement of sensor. This approach employs the step average between given domains for each sensor in all modes, despite being an interactive criterion. The location of sensors is determined by the high degree of freedom offered by ECOMAC. Eq. (9) gives the ECOMAC relation.

$$ECOMAC = \frac{\sum_{i=1}^{N\,M} |\{\varphi_i\} - \{\varphi_i^*\}|^2}{2NM} \tag{9}$$

This study evaluated the OSP of retrofitted and un-retrofitted slabs using the innovative Distributed-ECOMAC approach. The flowchart of this novel approach is shown in Fig. 2. The material properties of concrete and nanocomposite strips were selected based on experimental tests. The analysis of concrete slabs with and without strips was conducted using the NFEM. The results of the NFEM analysis, including mode shapes, were utilized to determine the modified distributed MAC, COMAC, and ECOMAC matrices. The results of the novel code called "FEMS-ECOMAC", designed and developed by the author of this paper, were used to optimize with a suitable genetic algorithm. Indeed, this code effectively identifies highly suitable points based on the DECOMAC approach, and the optimal number of sensors can be determined by the appropriate objective function. The procedures of IGA are shown in Fig. 2(b). The multi-objective function of IGA is given in Eq. (10).

$$\begin{aligned} f_1 &= w_1\left(1 - \sum_{h=1}^{z}(1 - modified\ ECOMAC_h)\right) \\ f_2 &= w_2(cost) \end{aligned} \tag{10}$$

Where, $(1 - \sum_{h=1}^{z}(1 - modified\ ECOMAC_h))$ and (cost) are the normalized objective function, and the sum of weights equals to $(\sum w_i = 1)$. The main problem with using this multi-objective function is to select the weight for each simulation. The $f1$ and $f2$ are very important in the optimization process to obtain the number and placement of sensors, so in this study the values of w_1 and w_2 were selected of 0.4 and 0.6 after undergoing numerous trial-error processes.

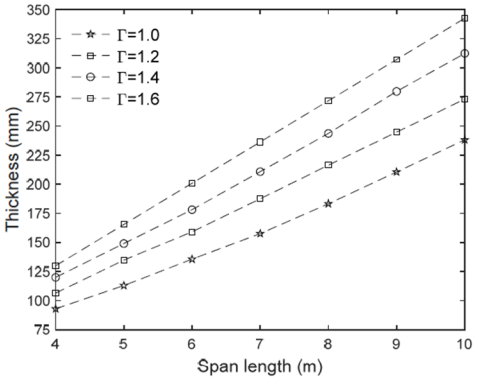

Fig. 3 The minimum slab thickness versus span length for various aspect ratio

Table 1 Specifications of concrete and nanocomposite

Material	E (Kg/m^2)	γ (Kg/m^3)	υ
Concrete	2738612000	2499	0.2
Nanocomposite	94410000000	3700	0.34

3.3 Validation of FEM analysis

The verification process was done based on a comparison between this study and the study of Vosoughifar and Manafi (2020). Statistical comparison between them shows that there is no significant difference (P-value < 0.05). To serve as case studies, concrete slabs of varying spans (5, 6, 7, and 8 meters) and ratios (1.0, 1.2, 1.4, and 1.6) were selected. For each of the slabs, both un-retrofitting and retrofitting scenarios with nanocomposite strips were considered, resulting in a total of 32 distinct cases evaluated to assess OSP patterns**.** The required slab thickness was obtained from the ACI code (2014) and these

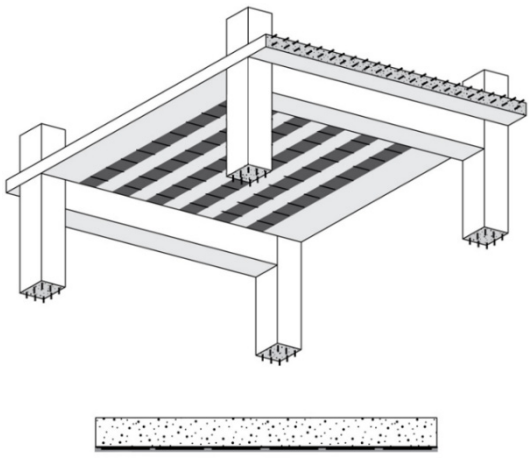

Fig. 4 Arrangement of nanocomposite strips in concrete slab

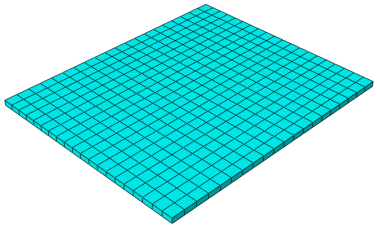

(a) Sample of optimized mesh

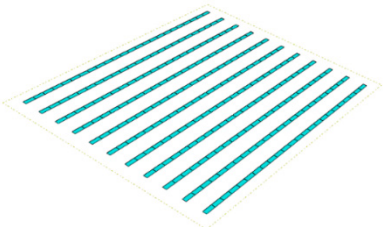

(b) Simulation nanocomposite strips in FE analysis

Fig. 5 Accurate mesh of a concrete slab

values relative to the slab span length for different aspect ratios are shown in Fig. 3.

Table 1 presents a summary of the materials used for the case studies.

The configuration of the nanocomposite strips, possessing a width of 10 cm and a thickness of 0.1 mm, is elucidated in Fig. 4. These strips are positioned at a center-to-center distance of 50 cm and are connected to the concrete slab.

In the Finite Element (FE) analysis, the optimal elements were attained by employing the trial-and-error approach for each case study. Figs. 5(a) and (b) illustrate the optimal mesh size samples for 5 m width and 5 m length and the simulation of nanocomposite strips in the FE process, respectively.

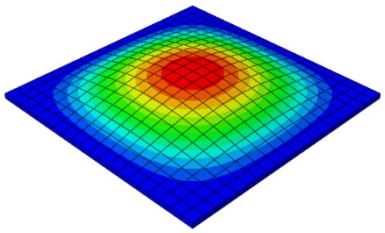

(a1) Frq = 8.0895 Hz

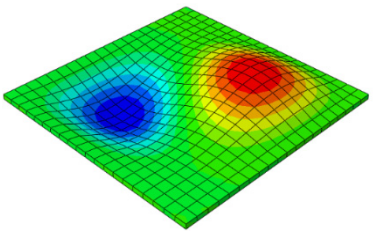

(a2) Frq = 11.303 Hz

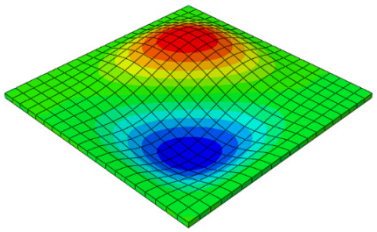

(a3) Frq = 15.680 Hz

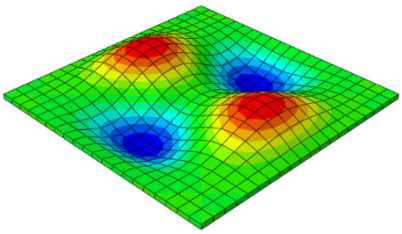

(a4) Frq = 16.107 Hz

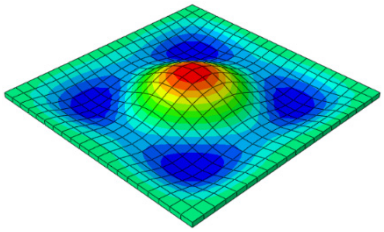

(a5) Frq = 20.198 Hz

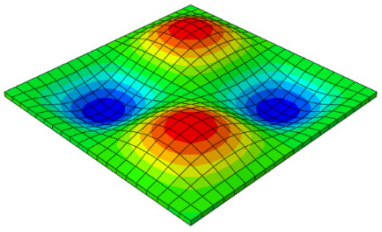

(a6) Frq =24.91 Hz

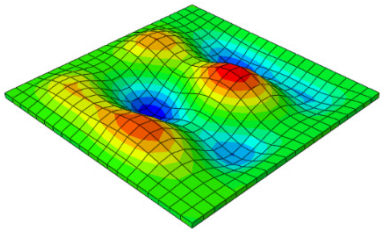

(a7) Frq = 26.528 Hz

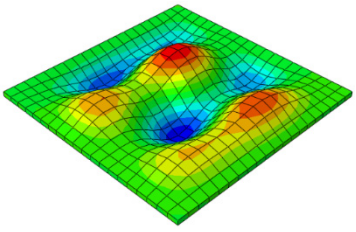

(a8) Frq = 27.039 Hz

Fig. 6(a) The effective mode shape of un-retrofitted slab with 5×5 dimension

3.4 FEM modal analysis

Modal analysis was carried out to achieve the OSP pattern of case studies. Figs. 6(a) and (b) depict the effective mode shapes of the slab, having dimensions of 5 m × 5 m, for the un-retrofitted and retrofitted categories, respectively.

The results of Fig. 6 show that un-retrofitted and retrofitted slabs have significant differences for all shapes. Consequently, frequency and mode shapes of un-retrofitted and retrofitted slabs in the first to the eighth modes were obtained for all case studies with aspect ratios of 1, 1.2, 1.4 and 1.6.

4. Results

The obtained mode shapes of all case studies were applied to calculate MAC, integrated COMAC and ECOMAC. The integrated COMAC and ECOMAC values should be used to obtain the OSP of slabs with the appropriate genetic algorithm. The initial OSP of slabs was determined by the highest topographic curvature of the IECOMAC curves. Essential processes to identify the placement of sensors were designed as a MATLAB toolbox called 'FEMS-ECOMAC'. As a result, comparative diagrams of sensor locations were attained by taking into account the coordinates' value and the distance from the origin for various slab modes, featuring different aspect ratios. The minimum number of modes, selected for acquiring the MAC matrix, should be significantly high such that the total effective mass of the model constitutes at least 90% of the actual mass according to building codes (ACI 2014). Figs. 7(a) and (b) show the 2D and 3D MAC values of an un-retrofitted 5×5 slab.

4.1 COMAC and ECOMAC contour Analysis

COMAC and ECOMAC values were determined using a distributed method based on line-by-line criteria. The Modal and integrated analysis results in selected concrete slabs were used to determine using COMAC, ECOMAC

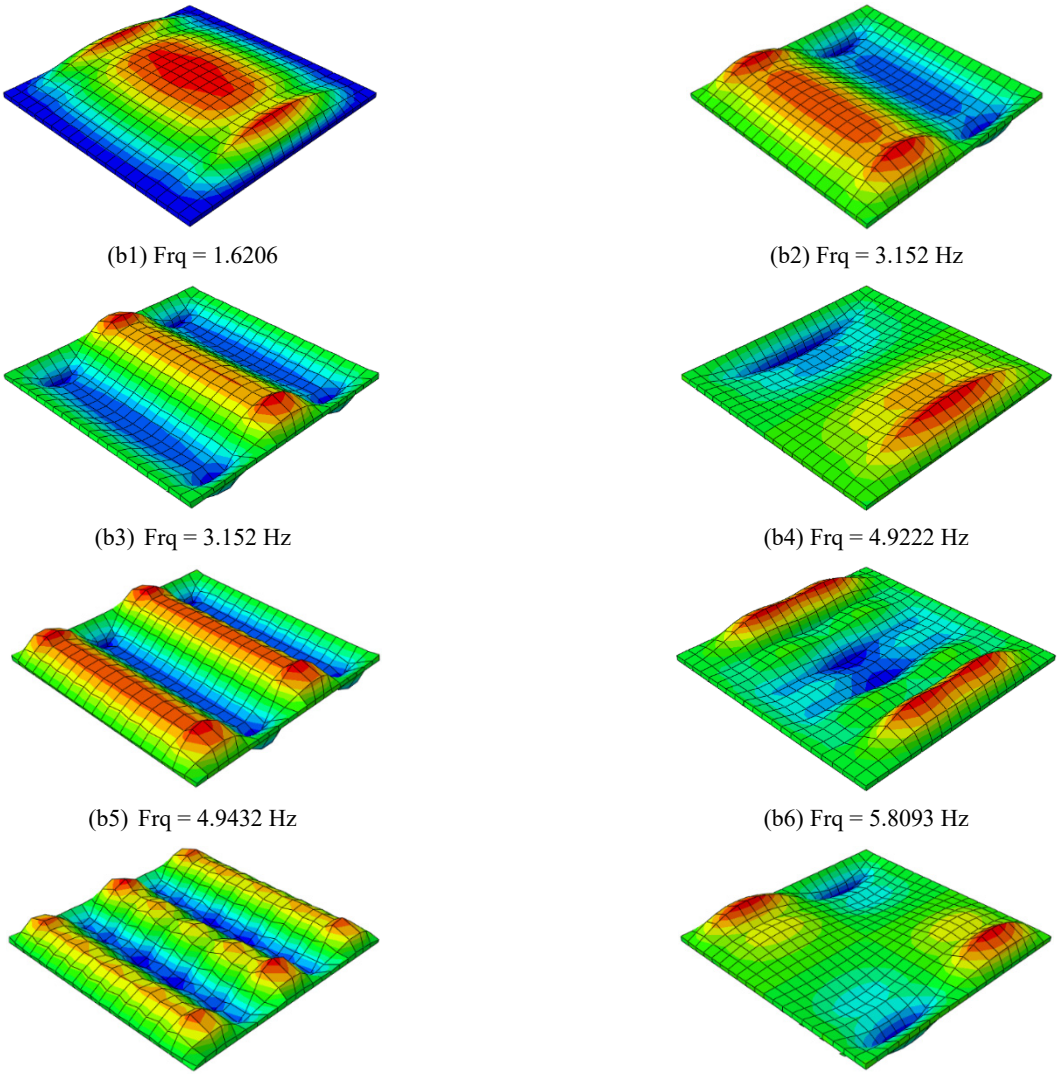

(b1) Frq = 1.6206 (b2) Frq = 3.152 Hz

(b3) Frq = 3.152 Hz (b4) Frq = 4.9222 Hz

(b5) Frq = 4.9432 Hz (b6) Frq = 5.8093 Hz

(b7) Frq = 6.9524 Hz (b8) Frq = 6.9524 Hz

Fig. 6 (b) The effective mode shape of retrofitted slab with 5×5 dimension

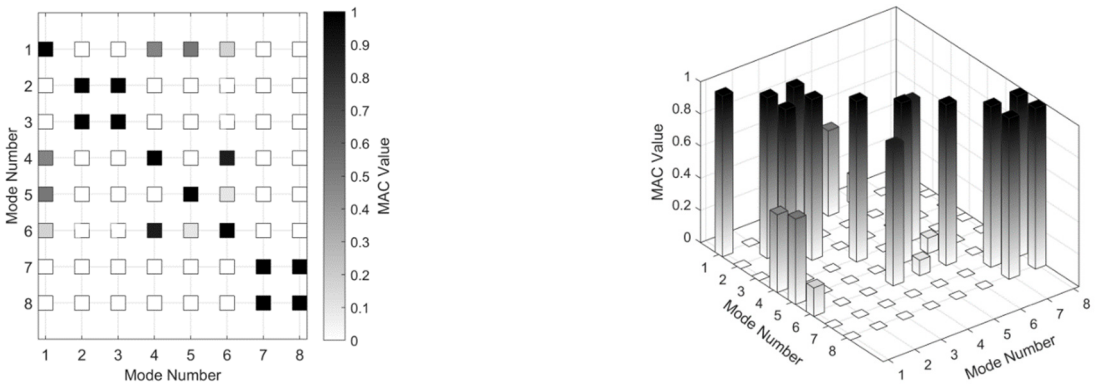

(a) 2D view (b) 3D view

Fig. 7 The MAC matrix for 5×5 un-retrofitted concrete slab

and their modified types. In this regard, NFEM results were classified as line-by-line information along the width of the slabs. The values of COMAC and ECOMAC were computed and the OSP for all lines were optimized based on the objective function and appropriate optimization process. Additionally, the traditional COMAC and ECOMAC approaches were modified to enhance the OSP. In this regard, the calculated values of COMAC and COMAC of slabs were utilized at each point to create COMAC and ECOMAC distributions. Distributed values of COMAC and ECOMAC for un-retrofitted and retrofitted slabs with nanostrips were calculated using the novel approach illustrated in Fig. 2. The modified COAMC contours for slabs with 5×5 dimensions are shown in Figs. 8(a) and (b). Additionally, the COMAC distributed contour for the concrete slab with a span length of 5 m and aspect ratio of 1.6 are shown in Fig. 9.

Figs. 8 and 9 illustrate a significant difference in modified-COMAC between un-retrofitted and retrofitted slabs. A statistical comparison between them demonstrates

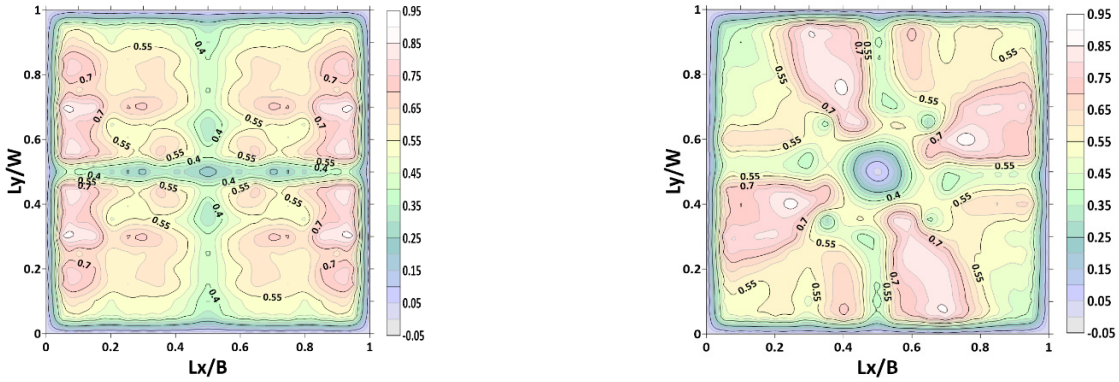

(a) Un-retrofitted slab (b) Retrofitted slab

Fig. 8 Modified COMAC contour for 5×5 slab (Λ = 1.0)

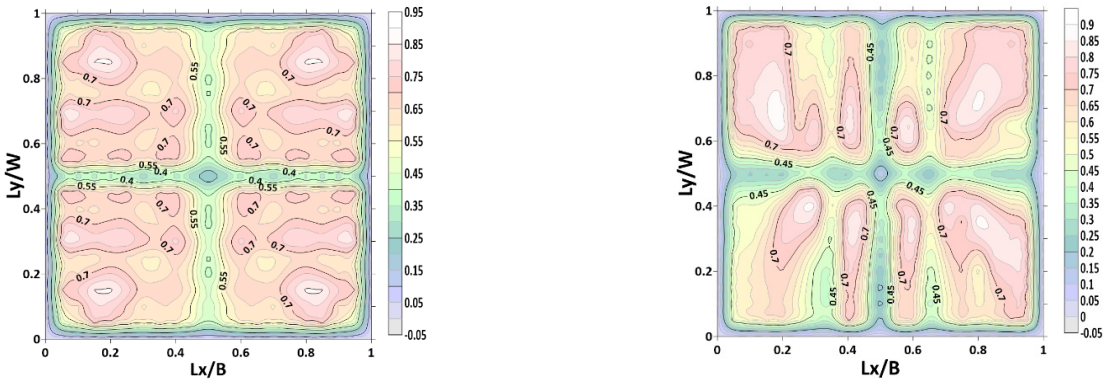

(a) Un-retrofitted slab (b) Retrofitted slab

Fig. 9 Modified COMAC contour for 5×8 dimension (Λ = 1.6).

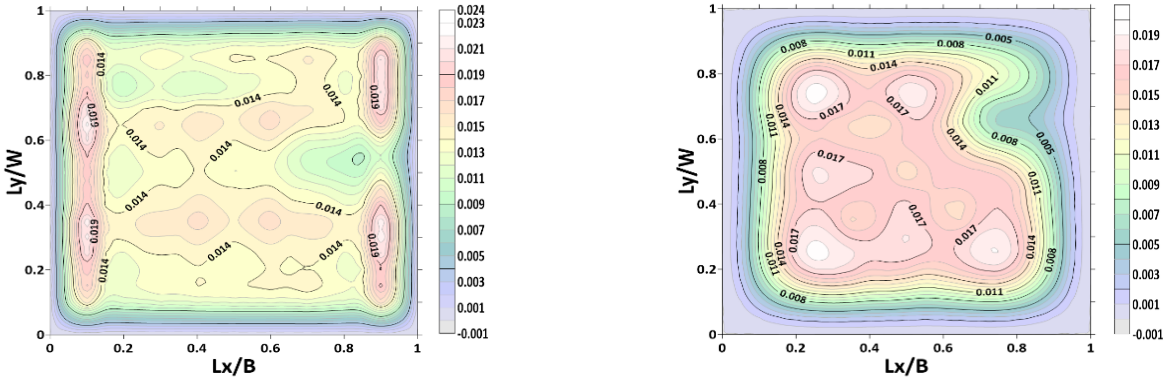

(a) Un-retrofitted slab (b) Retrofitted slab

Fig. 10 Modified ECOMAC contour for 5×5 dimension (Λ = 1.0)

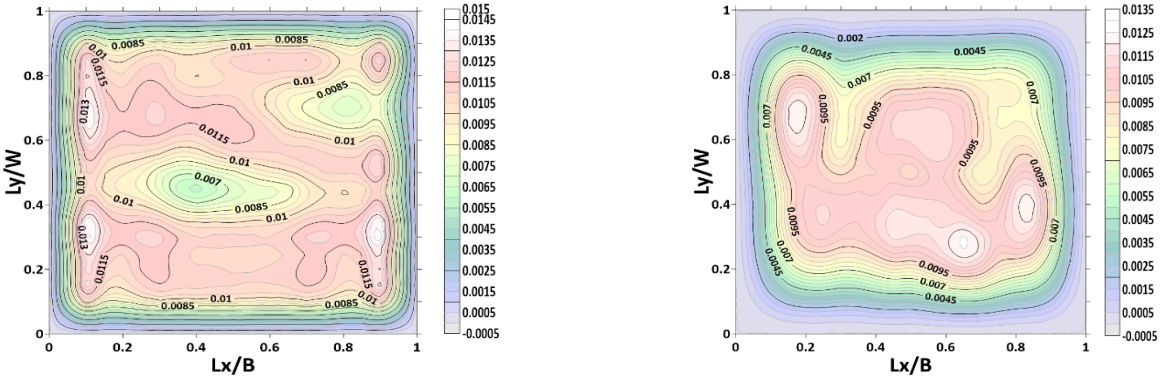

(a) Un-retrofitted slab (b) Retrofitted slab

Fig. 11 Modified ECOMAC contour for 5×8 dimension (Λ = 1.6)

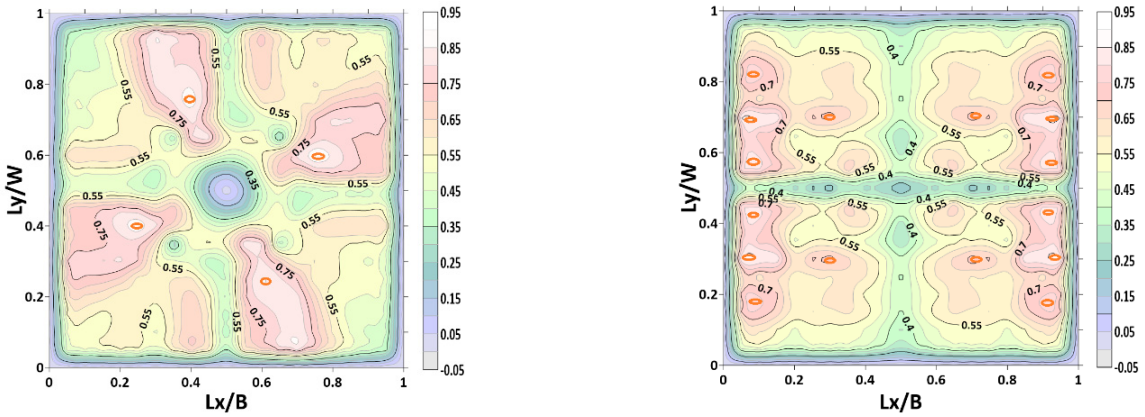

(a) Retrofitted slab (b) Un-retrofitted slab

Fig. 12 The OSP of slab based on COMAC approach

a complete change in the COMAC contours. The modified ECOAMC contours of un-retrofitted and retrofitted slabs for 5×5 dimensions are depicted in Figs. 10(a) and (b), respectively. Additionally, Fig. 11 exhibits distributed ECOMAC contours for concrete slabs with 5 m span lengths and aspect ratio of 1.6.

The results from the modified ECOMAC analysis demonstrate that the values for retrofitted slabs are significantly lower than those for un-retrofitted slabs. As a result, it can be inferred that the modified-ECOMAC approach is a more suitable criterion for determining the OSP of concrete slabs in comparison to the modified-COMAC approach.

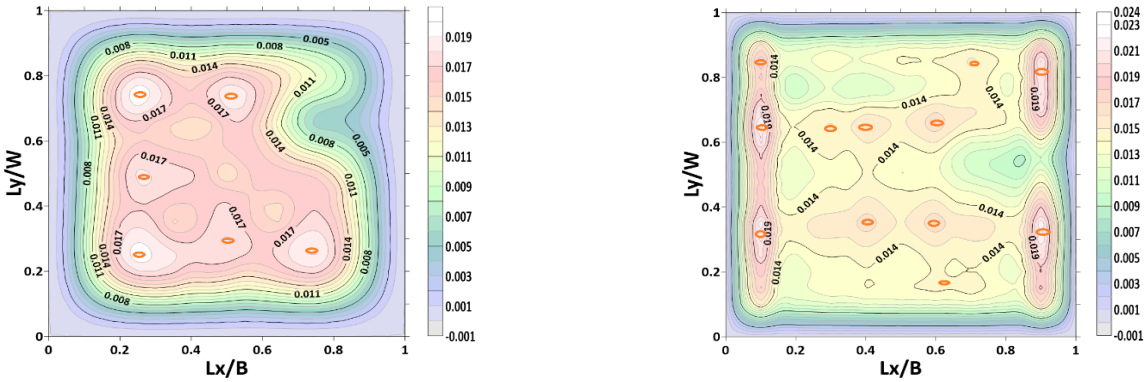

(a) Retrofitted slab (b) Un-retrofitted slab

Fig. 13 The OSP of slab based on ECOMAC approach

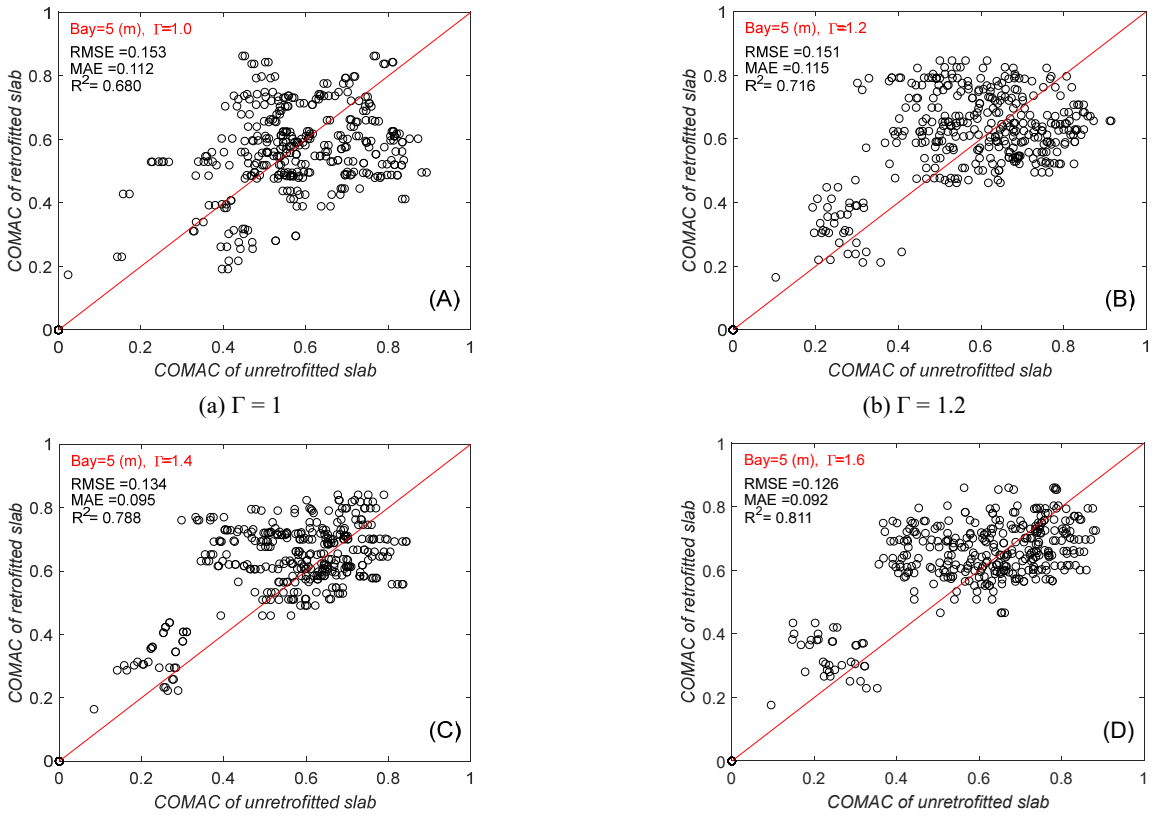

(a) Γ = 1 (b) Γ = 1.2

(c) Γ = 1.4 (d) Γ = 1.6

Fig. 14 Comparison the COMAC between retrofitted and un-retrofitted slab considering various Γ

4.2 OSP of slabs

OSP based on the distributed COMAC approach for both 5 m retrofitted and un-retrofitted slabs with $\Gamma = 1$, are shown in Fig. 12. It should be noted that sensor locations were obtained with COMAC values and appropriate optimization tools.

The results depicted in Fig. 12, along with corresponding values obtained for other slabs, clearly indicate that a slab with a span of 5 or 6 m would require approximately 3 to 5 sensors. On the other hand, for larger slabs such as those with a span of 7 to 8 m, around 6 to 8 sensors would be necessary. Notably, a comparison between Fig. 12(a) and (b) reveals that the number of sensors required for an un-retrofitted slab is greater than that needed for a retrofitted slab.

Furthermore, Fig. 13 displays the OSP of a slab with a 5 m span and Γ equal to 1, which was calculated by the ECOMAC approach, as well as the optimized tool for both retrofitted and un-retrofitted slabs.

The comparison of Figs. 12 and 13 clearly demonstrates a significant difference in sensor location obtained through COMAC and ECOMAC in both retrofitted and un-retrofitted slabs. Fig. 14 compares the COMAC values between retrofitted and un-retrofitted slabs for various amounts of Γ.

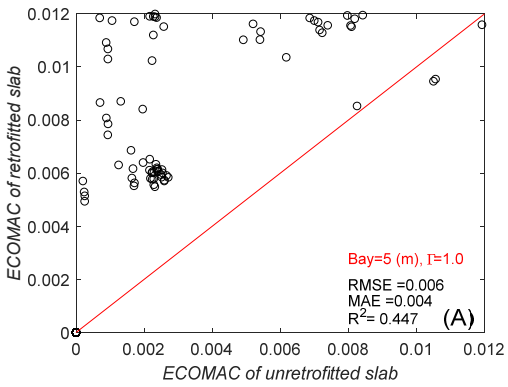

(a) Γ = 1

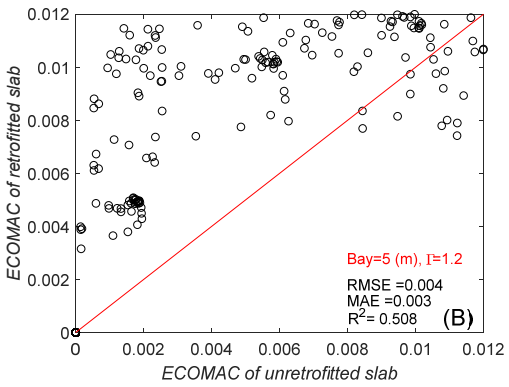

(b) Γ = 1.2

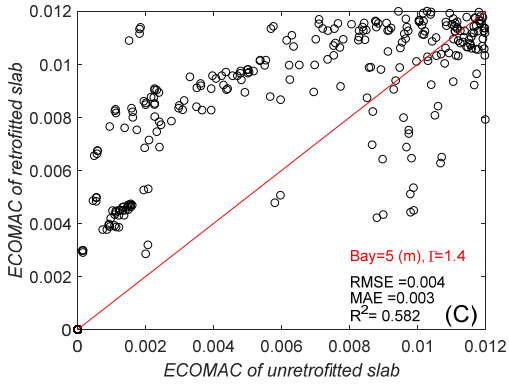

(c) Γ = 1.4

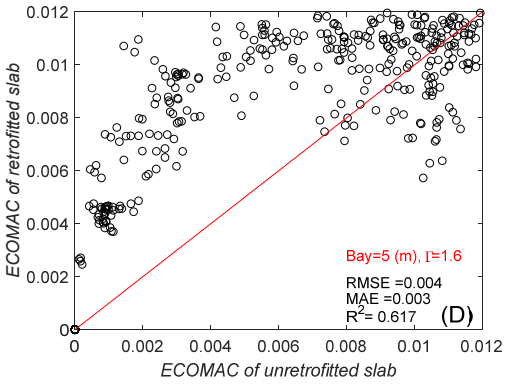

(d) Γ = 1.6

Fig. 15 Comparison the ECOMAC between retrofitted and un-retrofitted slab including various Γ

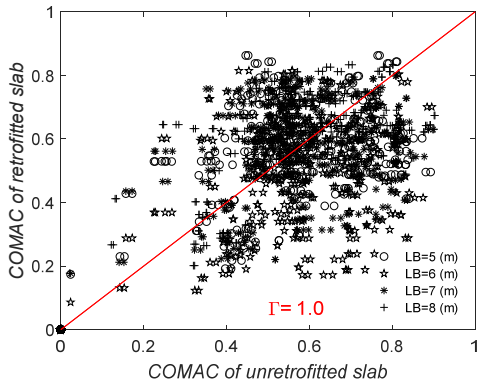

(a) Γ = 1

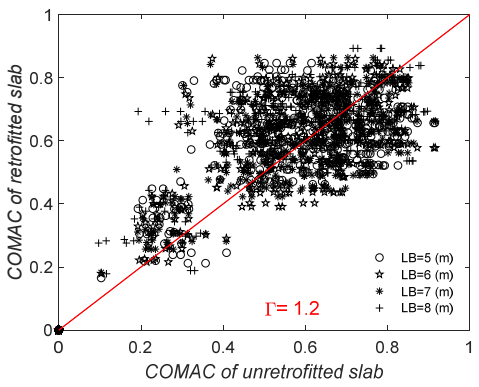

(b) Γ = 1.2

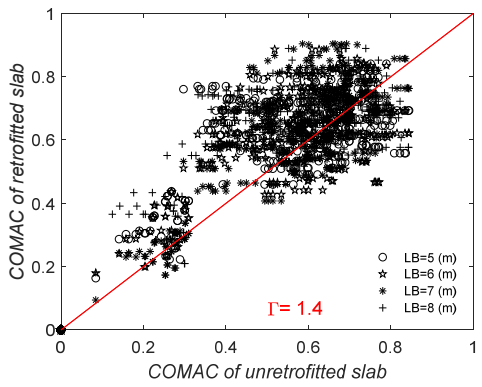

(c) Γ = 1.4

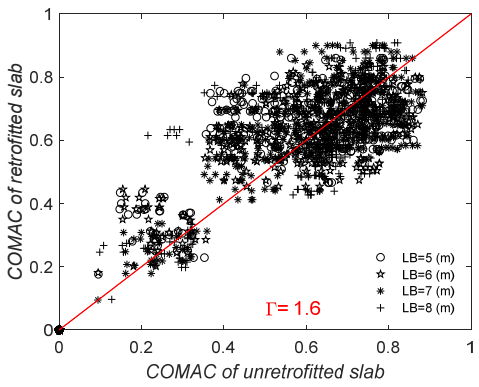

(d) Γ = 1.6

Fig. 16 Comparison the COMAC between retrofitted and un-retrofitted slab

Table 2 The average statistical comparison between retrofitted and un-retrofitted slabs based on COMAC analysis

Γ	MAE	RMSE	R^2
1	0.120	0.164	0.653
1.2	0.099	0.136	0.775
1.4	0.092	0.128	0.816
1.6	0.088	0.120	0.827

Table 3 The average statistical comparison between retrofitted and un-retrofitted slabs based on ECOMAC

Γ	MAE	RMSE	R^2
1	0.002	0.003	0.630
1.2	0.002	0.002	0.709
1.4	0.001	0.002	0.766
1.6	0.001	0.001	0.743

The results of Fig. 14 showed that the comparison of COMAC criteria between retrofitted and un-retrofitted slabs for Γ = 1.0 yielded a high MAE of 0.112, high RMSE of 0.153 and a low R^2 of 0.68. On the other hand, the comparison between them for Γ equal to 1.6 has a low MAE of 0.092, low RMSE of 0.126 and a high R^2 of 0.811. The comprehensive findings suggest that as the slab width increases, the COMAC values for both retrofitted and un-retrofitted items will remain closely comparable, provided that the length of the bay remains constant for all slabs.

Fig. 15 compares the ECOMAC values between retrofitted and un-retrofitted slabs for various amounts of Γ.

The comparison of ECOMAC values between retrofitted and un-retrofitted slabs for various Γ based on Fig. 15 reveals a substantial difference between them. Statistical metrics indicate that for Γ equal to 1, there is a high MAE of 0.004, a high RMSE of 0.006, and a low R^2 of 0.447. The results demonstrate that as the slab width increases, the ECOMAC values for retrofitted and un-retrofitted slabs converge, as long as the bay length remains constant. However, a significant difference between them persists even in this scenario. Therefore, to obtain an accurate solution, the OSP calculated using the ECOMAC approach must consider the different parameters between neighboring elements.

Fig. 16 illustrates the scatter plot of COMAC value between retrofitted and un-retrofitted slabs with varying LB and Γ. This figure encompasses all grids in the case studies, facilitating a comprehensive comparison of the two slab states. Table 2 presents the average statistical comparison of the COMAC for different LBs between the retrofitted and un-retrofitted slab modes. The comparison provides a thorough analysis of the effectiveness of the retrofitting process.

The results of Fig. 16 show that the comparison of COMAC criteria between retrofitted and un-retrofitted slabs for Γ = 1.0 has a highest RMSE of 0.164 and a highest MAE of 0.120 and lowest R^2 of 0.653 between slabs. In

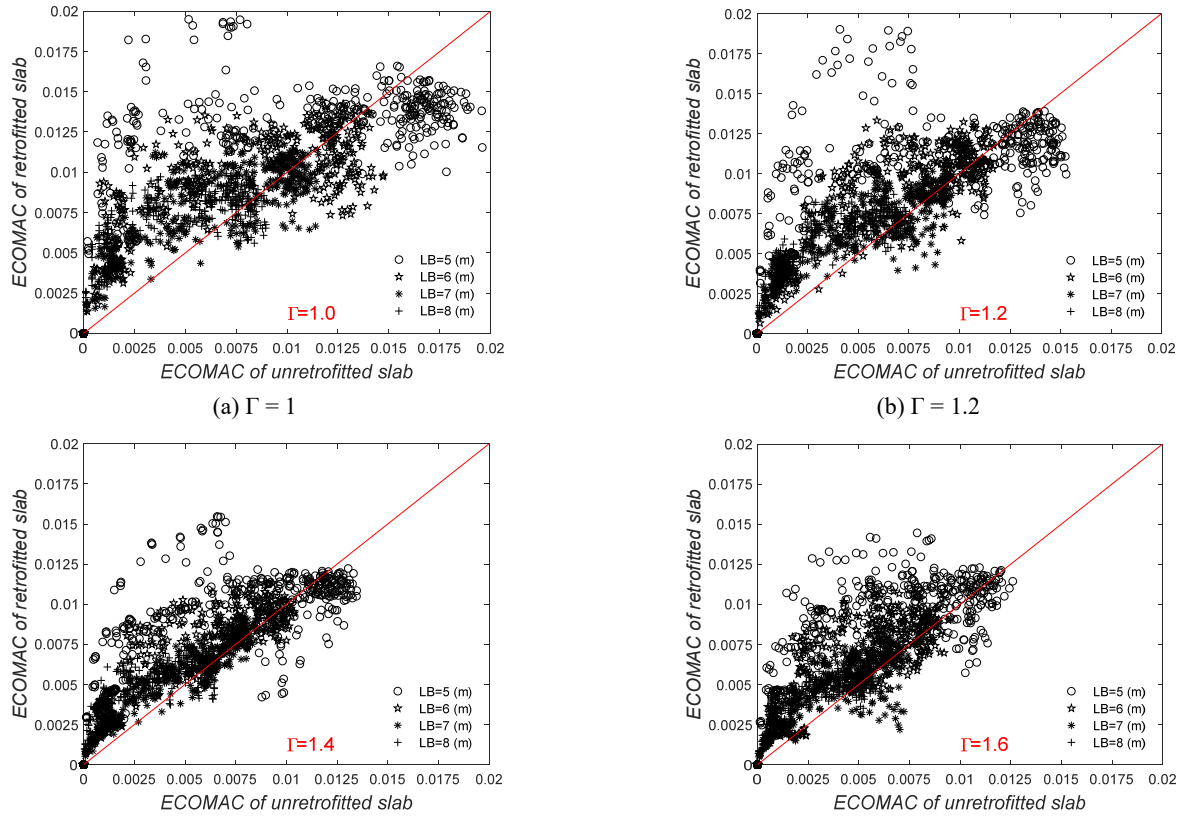

(a) Γ = 1 (b) Γ = 1.2

(c) Γ = 1.4 (d) Γ = 1.6

Fig. 17 Comparison the ECOMAC between retrofitted and un-retrofitted slabs

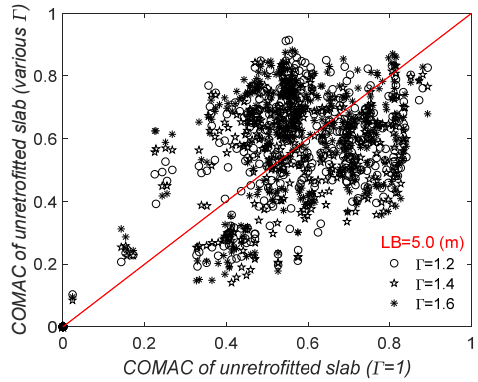

(a) Un-retrofitted slabs

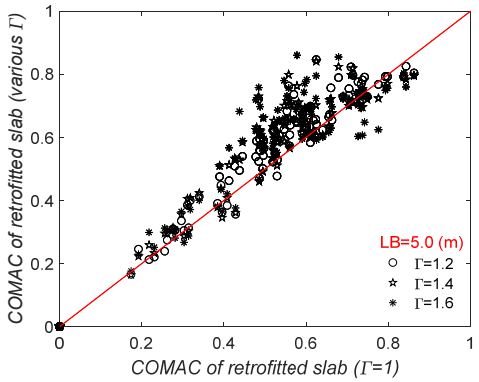

(b) Retrofitted slabs

Fig. 18 Comparison of COMAC sensor location including various Γ for LB = 5

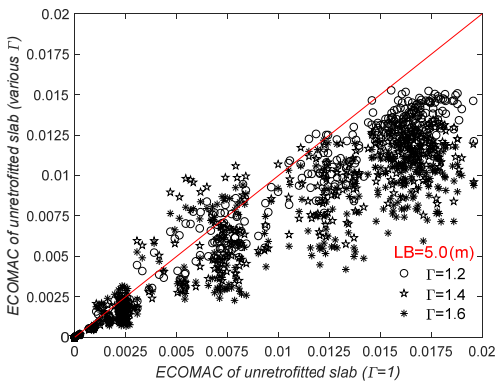

(a) Un-retrofitted slabs

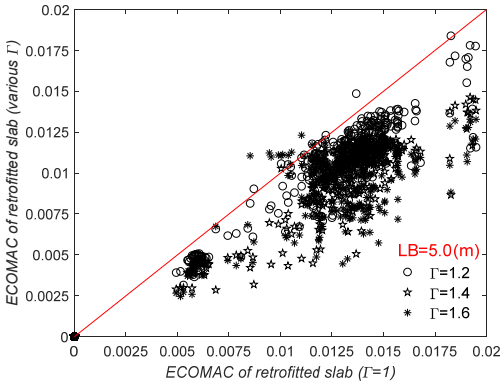

(b) Retrofitted slabs

Fig. 19 Comparison of ECOMAC sensor location including various Γ for LB = 5

Table 4 The statistical comparison between retrofitted and un-retrofitted slabs based on COMAC analysis

Γ	MAE	RMSE	R^2	Slab
1.2	0.046	0.066	0.962	Retrofitted
1.4	0.059	0.082	0.938	Retrofitted
1.6	0.074	0.103	0.897	Retrofitted
1.2	0.132	0.168	0.643	Unretrofitted
1.4	0.127	0.163	0.650	Unretrofitted
1.6	0.136	0.178	0.620	Unretrofitted

Table 5 The statistical comparison between retrofitted slabs based on ECOMAC analysis

Γ	MAE	RMSE	R^2	LB
1.2	0.002	0.002	0.953	Retrofitted
1.4	0.003	0.003	0.929	Retrofitted
1.6	0.003	0.004	0.866	Retrofitted
1.2	0.002	0.002	0.968	Unretrofitted
1.4	0.003	0.004	0.911	Unretrofitted
1.6	0.003	0.005	0.852	Unretrofitted

addition, for Γ = 1.2 the statistical results show that case studies have a high RMSE of 0.136 and a MAE of 0.099 and a low R^2 of 0.775 between slabs. The overall results reveal that with an increase in slab width, the COMAC values for the retrofitted and un-retrofitted slabs tend to converge. Scatter plots of ECOMAC values between retrofitted and un-retrofitted slabs with different LB and Γ are shown in Fig. 17. The average statistical comparison of ECOMAC including different LBs between the two slab modes is given in Table 3.

The results of Fig. 17 and Table 3 indicated that Γ = 1.0 situation, has a high RMSE of 0.003 and a high MAE of 0.002 and a low R^2 of 0.630 among slabs. The outcomes of this figure clearly depict a converging trend in ECOMAC values for both retrofitted and un-retrofitted slabs, as the slab width progressively increases. This tendency is further corroborated by the COMAC results. Fig. 18 compares COMAC values in retrofitted and un-retrofitted slabs with considering various aspect ratios. Table 4 summarizes the statistical differences between retrofitted and un-retrofitted slabs.

The scatter plot depicting COMAC values for retrofitted and un-retrofitted slabs of varying aspect ratios based on Fig. 18 clearly indicates a robust agreement between them. Moreover, there is a low MAE of 0.046 and low RMSE of 0.066 and a high R^2 in average for the retrofitted slabs. These findings are further supported by the statistical analysis presented in Table 4, which highlights the superior

performance of retrofitted slabs compared to un-retrofitted slabs. Fig. 19 compares ECOMAC values in retrofitted and un-retrofitted slabs on various aspect ratios.

Table 5 represents the statistical differences between retrofitted and un-retrofitted slabs. This table shows that there is no significant difference between retrofitted and un-retrofitted slabs based on the ECOMAC analysis. Based on the obtained results, a conclusive inference can be drawn that the retrofitted slab exhibits a significantly lower statistical error rate compared to the un-retrofitted slab. Additionally, the value of R^2 in the retrofitted slab is observed to be substantially higher than that of the un-retrofitted slab. It is also observed that for slabs with larger aspect ratios for spans of 5, 6, 7, and 8 meters, the error rate is comparatively lower, thereby indicating no significant difference between them. The overall findings of the study suggest that the statistical error rate in the COMAC approach is relatively higher than that of the ECOMAC method. However, the difference in the error rates between the two approaches is not significant.

5. Conclusions

The utilization of SHM provides a highly efficient means to ensure the safety of structures. However, this process is limited due to the cost of the sensor system and the coverage intensity of the sensors (Firoozbakht *et al*. 2019), allowing only a restricted number of sensors to be employed. Optimal Sensor Placement (OSP) is crucial for ensuring precise monitoring in terms of both reliability and cost optimization for start-up sensors. Moreover, OSP facilitates the identification of structural vulnerabilities by identifying the most suitable locations for sensor placement. The present study aimed to assess the OSP of retrofitted concrete slabs utilizing NPS. To achieve this objective, the appropriate nonlinear FEM and OSP approach was designed based on the ECOMAC method as a toolbox of MATLAB called the DECOMAC approach, by the authors of this paper. This approach uses distributed ECOMAC analysis instead of line-by-line approach that is evaluated by Ercan and Papadimitriou (2021), Kaveh and Dadras Eslamlou (2019), Tan and Zhang (2020) and Vosoughifar and Manafi (2020). The primary advantage of this innovative approach is its capacity to pinpoint the precise location of sensors by utilizing distributed analysis, in contrast to current methods. The results show that while slab width increases, the COMAC values for the retrofitted and un-retrofitted slabs remain close to each other with respect to the fact that the length of the bay is constant for all slabs. Statistical comparison of DECOMAC criteria between retrofitted and un-retrofitted slabs for aspect ratio 1, shows that there are high values RMSE, MAE and low values R^2 of 0.164, 0.120 and 0.653, respectively. Furthermore, for the aspect ratio 1.2 the statistical results show that that there is a high RMSE, MAE and low R^2 values of 0.136, 0.099 and 0.775, respectively. Therefore, significant differences were observed for statistical errors and R^2 between aspect ratios 1 and 1.2 compared to other ratios.

The results indicated that the ECOMAC values for retrofitted and un-retrofitted slabs remain close to each other while the slab width increases. It can be inferred that the statistical error rate associated with the COMAC and ECOMAC methods is higher compared to the DECOMAC approach, which means that the DECOMAC method performs better in the OSP of slabs. Thus, the modified DECOMAC approach can detect the problems of OSP more accurately than the current COMAC and COMAC methods. Therefore, the OSP obtained using the DECOMAC method is a better solution due to the simultaneous consideration of adjacent elements according to the distributed method. As a consequence, both designers and owners of concrete slabs should regard the DECOMAC method as a viable option to accurately determine the sensor location's effectiveness.

This study focused on the importance of SHM of two-way reinforced concrete slabs using NPS as external reinforcement. The MATLAB toolbox named DECOMAC was developed to optimize the process of sensor placement using a nonlinear FEM approach and a multi-objective function based on the distributed ECOMAC method. The study considered case studies of concrete slabs with different aspect ratios and found that the optimized sensor placement by the DECOMAC algorithm showed a significant difference between un-retrofitted and retrofitted slabs.

References

ACI 318 (2014), Building Code Requirements for Reinforced Concrete and Commentary, American Concrete Institute, ACI Committee 318; Farmington Hills, IL, USA, 348.

Afefy, H.M., Baraghith, A.T and Mahmoud, M.H. (2019), "Retrofitting of defected reinforced-concrete cantilever slabs using different techniques", *Mag. Concr. Res.*, **72**(14), 703-719. https://doi.org/10.1680/jmacr.18.00340

Bekas, D., Grammatikos, S.A., Kouimtzi, C. and Paipetis, A.S. (2015), "Linear and non-linear electrical dependency of carbon nanotube reinforced composites to internal damage", *IOP Conference Series: Materials Science and Engineering*. https://doi.org/10.1088/1757-899X/74/1/012002

Coppolino, R.N. and Rubin, S. (1980), "Detectability of structural failures in offshore platforms by ambient vibration monitoring", *Proceedings of the 12th Annual Offshore Technology Conference*, pp. 101-110.

Ercan, T. and Papadimitriou, C. (2021), "Optimal sensor placement for reliable virtual sensing using modal expansion and information theory", *Sensors*, **21**(10), 3400. https://doi.org/10.3390/s21103400

Eringen, A.C. and Edelen, D.G.B. (1972), "On nonlocal elasticity", *Int. J. Eng. Sci.*, **10**, 233-248. https://doi.org/10.1016/0020-7225(72)90039-0

Fernandes, H., Lúcio, V. and Ramos, A. (2017), "Strengthening of RC slabs with reinforced concrete overlay on the tensile face", *Eng. Struct.*, **132**, 540-550. https://doi.org/10.1016/j.engstruct.2016.10.011

Firoozbakht, M., Vosoughifar, H. and Ghari Ghoran, A. (2019), "Coverage intensity of optimal sensors for common, isolated, and integrated steel structures using novel approach of FEM-MAC-TTFD", *Int. J. Distrib. Sens. Netw.* https://doi.org/10.1177/1550147719857568

Guo, Z., Xu, Z. and Chen, C. (2017), "Behavior of GFRP retrofitted reinforced concrete slabs subjected to conventional explosive blast", *Mater. Struct.*, **50**, 236. https://doi.org/10.1617/s11527-017-1107-6

Herraiz, B. and Vogel, T. (2016), "Novel design approach for the

analysis of laterally unrestrained reinforced concrete slabs considering membrane action", *Eng. Struct.*, **123**, 313-329. https://doi.org/10.1016/j.engstruct.2016.05.033

Hunt, D.L., Weiss, S.P., West, W.M., Dunlap, T.A. and Freemeyer, S.R. (1990), "Development and implementation of a shuttle modal inspection system", *Sound Vib.*

Kang, I., Schulz, M.J., Kim, J.H., Shanov, V. and Shi, D. (2006), "A carbon nanotube strain sensor for structural health monitoring", *Smart Mater. Struct.*, **15**, 737. https://doi.org/10.1088/0964-1726/15/3/009

Kaveh, A., Talaei, A.S. and Nasrollahi, A. (2016), "Application of Probabilistic Particle Swarm in Optimal Design of Large-Span Prestressed Concrete Slabs", *Iran. J. Sci. Technol. Trans. Civil Eng.*, **40**, 33-40. https://doi.org/10.1007/s40996-016-0005-4

Kaveh, A. and Dadras Eslamlou, A. (2019), "An efficient two-stage method for optimal sensor placement using graph-theoretical partitioning and evolutionary algorithms", *Struct. Health Monit.*, **26**, e2325. https://doi.org/10.1002/stc.2325

Kaveh, A., Dadras Eslamlou, A., Rahmani, P. and Amirsoleimani, P. (2022), "Optimal sensor placement in large-scale dome trusses via Q-learning-based water strider algorithm", *Struct. Control Health Monit.*, **29**(7), e2949. https://doi.org/10.1002/stc.2949

Khajehdehi, R. and Panahshahi, N. (2016), "Effect of openings on in-plane structural behavior of reinforced concrete floor slabs", *J. Build. Eng.*, **7**, 1-11. https://doi.org/10.1016/j.jobe.2016.04.011

Konka, H.P., Wahab, M.A. and Lian, K. (2013), "Piezoelectric fiber composite transducers for health monitoring in composite structures", *Sens. Actuator A Phys.*, **194**, 84-94. https://doi.org/10.1016/j.sna.2012.12.039

Lu, S., Tian, C., Wang, X., Zhang, L., Du, K., Ma, K. and Xu, T. (2018), "Strain sensing behaviors of GnPs/epoxy sensor and health monitoring for composite materials under monotonic tensile and cyclic deformation", *Compos. Sci. Technol.*, **158**, 94-100. https://doi.org/10.1016/j.compscitech.2018.02.017

Ma, C., Wang, D. and Wang, Z. (2017), "Seismic retrofitting of full-scale RC interior beam-column-slab subassemblies with CFRP wraps", *Compos. Struct.*, **159**, 397-409. https://doi.org/10.1016/j.compstruct.2016.09.094

Maheri, M.R., Khajeheian, M.K. and Vatanpour, F. (2019), "In-plane seismic retrofitting of hollow concrete block masonry walls with RC layers", *Structures*, **20**, 425-436. https://doi.org/10.1016/j.istruc.2019.05.008

Mosalam, K.M. and Mosallam, A.S. (2001), "Nonlinear transient analysis of reinforced concrete slabs subjected to blast loading and retrofitted with CFRP composites", *Compos. B. Eng.*, **32**(8), 623-636. https://doi.org/10.1016/S1359-8368(01)00044-0

Navarro, M., Ivorra, S. and Varona, F.B. (2018), "Parametric computational analysis for punching shear in RC slabs", *Eng. Struct.*, **165**, 254-263. https://doi.org/10.1016/j.engstruct.2018.03.035

Sengezer, E. and Seidel, G. (2017), "Structural Health Monitoring of Nanocomposite Bonded Energetic Materials Through Piezoresistive Response", *AIAA J.*, **56**, 1-14. https://doi.org/10.2514/1.J056178

Shokouhi, S.K. and Vosoughifar, H. (2013), "Optimal sensor placement in the lightweight steel framing structures using the novel TTFD approach subjected to near-fault earthquakes", *J. Civil Struct. Health Monit.*, **3**, 257-267. https://doi.org/10.1007/s13349-013-0053-4

Tan, Y. and Zhang, L. (2020), "Computational methodologies for optimal sensor placement in structural health monitoring: A review", *Struct. Health Monit.*, **19**(4), 1287-1308. https://doi.org/10.1177/1475921719877579

Tan, A.C., Cha, J.J.Y. and Kang, I. (2011), "Novel corrosion sensor based on carbon nanotube composites for structural health monitoring", *Proceedings of the Thermal and Materials Nanoscience and Nanotechnology for Structural Health Monitoring*, Antalya, Turkey, Begell House, pp. 1-7. http://dx.doi.org/10.1615/ICHMT.2011.TMNN-2011.70

Thiagarajan, G., Kadambi, A.V., Robert, S. and Johnson, C.F. (2015), "Experimental and finite element analysis of doubly reinforced concrete slabs subjected to blast loads", *Int. J. Impact Eng.*, **75**, 162-173. https://doi.org/10.1016/j.ijimpeng.2014.07.018

Vandiver, J.K. (1977), "Detection of structural failure on fixed platforms by measurement of dynamic response", *J. Pet. Technol.*, 305-310. https://doi.org/10.4043/2267-MS

Vosoughifar, H. and Khorani, M. (2019), "Optimal Sensor Placement of RCC Dam using Modified Approach of COMAC-TTFD", *KSCE J. Civil Eng.*, **23**, 2933-2947. https://doi.org/10.1007/s12205-019-0716-8

Vosoughifar, H. and Manafi, P. (2020), "Sensor location in concrete slabs with various layout of opening using modified 'FEMS-COMAC' approach", *Earthq. Eng. Eng. Vib.*, **19**, 205-222. https://doi.org/10.1007/s11803-020-0557-y

Vosoughifar, H., Shokouhi, S.K. and Farshadmanesh, P. (2012), "Optimal sensor placement of steel structure with UBF system for SHM using hybrid FEM-GA technique", *Civil Structural Health Monitoring Workshop*. http://creativecommons.org/licenses/by/3.0/

Wang, W. (2013), "Towards structural health monitoring in carbon nanotube reinforced composites", Bachelor's Thesis; Massachusetts Institute of Technology, Department of Materials Science and Engineering.

Wang, G., Wang, Y., Zhang, P., Zhai, Y., Luo, Y., Li, L. and Luo, S. (2018), "Structure dependent properties of carbon nanomaterials enabled fiber sensors for in situ monitoring of composites", *Compos. Struct.*, **195**, 36-44. https://doi.org/10.1016/j.compstruct.2018.04.052

Yi, T.H., Zhou, G.D., Li, H.N. and Wang, C.W. (2016), "Optimal placement of triaxial sensors for modal identification using hierarchic wolf algorithm", *Struct. Health Monit.*, **24**(8). https://doi.org/10.1002/stc.1958

HJ